© 2014. Published by The Company of Biologists Ltd | Journal of Cell Science (2014) 127, 216–229 doi:10.1242/jcs.136580

RESEARCH ARTICLE

Pain modulators regulate the dynamics of PKA-RII phosphorylation in subgroups of sensory neurons

Joerg Isensee[1,2,*], Mandy Diskar[3], Steffen Waldherr[4], René Buschow[1,2,5], Jan Hasenauer[6,7], Anke Prinz[3], Frank Allgöwer[6], Friedrich W. Herberg[3] and Tim Hucho[1,2]

ABSTRACT

Knowledge about the molecular structure of protein kinase A (PKA) isoforms is substantial. In contrast, the dynamics of PKA isoform activity in living primary cells has not been investigated in detail. Using a high content screening microscopy approach, we identified the RIIβ subunit of PKA-II to be predominantly expressed in a subgroup of sensory neurons. The RIIβ-positive subgroup included most neurons expressing nociceptive markers (TRPV1, NaV1.8, CGRP, IB4) and responded to pain-eliciting capsaicin with calcium influx. Isoform-specific PKA reporters showed in sensory-neuron-derived F11 cells that the inflammatory mediator PGE_2 specifically activated PKA-II but not PKA-I. Accordingly, pain-sensitizing inflammatory mediators and activators of PKA increased the phosphorylation of RII subunits (pRII) in subgroups of primary sensory neurons. Detailed analyses revealed basal pRII to be regulated by the phosphatase PP2A. Increase of pRII was followed by phosphorylation of CREB in a PKA-dependent manner. Thus, we propose RII phosphorylation to represent an isoform-specific readout for endogenous PKA-II activity *in vivo*, suggest RIIβ as a novel nociceptive subgroup marker, and extend the current model of PKA-II activation by introducing a PP2A-dependent basal state.

KEY WORDS: Protein kinase A, RII phosphorylation, cAMP response element-binding protein, Nociception, Sensitization

INTRODUCTION

Protein kinase A (PKA) represents a family of tetrameric kinases composed of regulatory (R) and catalytic (C) subunits. At low cAMP concentrations, PKA is maintained as an inactive R_2C_2 holoenzyme. Binding of cAMP to R-subunits induces the dissociation of the holoenzyme complex and release of C-subunits facilitating substrate phosphorylation (Taylor et al., 1990). Four regulatory (RIα, RIβ, RIIα, RIIβ) and four catalytic subunits (Cα, Cβ, Cγ, PrKX) give rise to multiple isoenzymes, categorized by their R-subunit class into PKA-I and PKA-II, respectively. These isoenzymes differ in their biochemical properties, expression pattern, interacting proteins, as well as their subcellular localization (Pidoux and Taskén, 2010). Also, large variations in the quaternary structure of PKA-holoenzyme complexes have been described (Boettcher et al., 2011; Kim et al., 2007; Vigil et al., 2006; Wu et al., 2007; Zhang et al., 2012). One difference between PKA-I and PKA-II is in their inhibitory domain, which blocks the catalytic subunit. Whereas RI subunits block the C-subunits by a non-phosphorylatable pseudosubstrate, RII subunits carry a serine within that inhibitory domain rendering them substrates of C-subunits. Recently, the analysis of cell homogenates and protein crystals suggested that RII subunits are fully phosphorylated already in the inactive PKA-II complex (Manni et al., 2008; Zhang et al., 2012). However, whether this also applies to PKA-II in intact cells *in vivo* has not been conclusively investigated so far.

Knockout studies show that R-subunit isoforms are not functionally redundant (Amieux et al., 2002; Brandon et al., 1998; Cummings et al., 1996; Fischer et al., 2004; Huang et al., 1995; Rao et al., 2004; Thiele et al., 2000). However, knockouts of R-subunits have limitations in revealing specific functions of PKA isoforms. Loss of one of the R-subunit isoforms might induce compensatory upregulation of other regulatory isoforms or result in increased free catalytic subunits, leading to uncontrolled excessive PKA activity (Amieux et al., 1997; Amieux et al., 2002). Therefore, isoform-specific reporter constructs have been designed to analyze the differential involvement of PKA isoforms in cellular functions (Prinz et al., 2006a). These approaches, however, require transfection of cells and therefore cannot be applied to many heterogeneous primary cell models. Thus, novel approaches are required to be able to evaluate the regulation and activity of endogenous PKA isoforms in wild-type cells.

Endogenous isoform-specific reporters of PKA activity are of crucial importance for the analysis of adult nociceptive neurons, which are highly heterogeneous and difficult to transfect. Nociceptive neurons react to intense thermal, mechanical or chemical stimuli and thereby initiate the feeling of pain (Basbaum et al., 2009). They can be sensitized by various inflammatory mediators including agonists of $G\alpha_s$-coupled GPCRs activating the PKA pathway (Hucho and Levine, 2007). Indeed, PKA represents an indirect target of common pain medications such as opioids and non-steroidal anti-inflammatory drugs (NSAIDs) (Pierre et al., 2009). PKA phosphorylates and sensitizes ion channels such as the voltage-gated sodium channel NaV1.8 and the transient receptor potential channel TRPV1, which are crucial for the functionality of nociceptive neurons (Bhave et al., 2002; England et al., 1996; Fitzgerald et al., 1999; Jeske et al., 2008; Rathee et al., 2002; Wang et al., 2007; Zhang et al., 2008). Moreover, activation of the cAMP response-element-binding

[1]University Hospital Cologne, Department of Anesthesiology and Intensive Care Medicine, Experimental Anesthesiology and Pain Research, Robert Koch Str. 10, 50931 Cologne, Germany. [2]Department for Human Molecular Genetics, Max Planck Institute for Molecular Genetics, Ihnestrasse 73, 14195 Berlin, Germany. [3]University of Kassel, Department of Biochemistry, Heinrich-Plett-Str. 40, 34132 Kassel, Germany. [4]Institute for Automation Engineering, Otto-von-Guericke-Universität Magdeburg, Universitätsplatz 2, 39106 Magdeburg, Germany. [5]Institute of Chemistry and Biochemistry, Freie Universität Berlin, Takustr. 3, 14195 Berlin, Germany. [6]Institute for Systems Theory and Automatic Control, University of Stuttgart, Pfaffenwaldring 9, 70550 Stuttgart, Germany. [7]Institute of Computational Biology, Helmholtz Center Munich, Ingolstädter Landstr. 1, 85764 Neuherberg, Germany.

*Author for correspondence (joerg.isensee@uk-koeln.de)

Received 10 June 2013; Accepted 9 October 2013

Journal of Cell Science

Journal of Cell Science (2014) 127, 216–229 doi:10.1242/jcs.136580

protein (CREB) may occur downstream of PKA to induce gene expression required for long-term sensitization (Ji et al., 2003). Although most PKA studies in the context of pain have not taken into account the different isoforms, knockout of the RIβ subunit indicated a small but significant involvement of PKA-I (Malmberg et al., 1997). Whether PKA-II also is activated in nociceptive neurons in response to inflammatory mediators is unknown.

We set out to identify subgroup-specific expression of PKA regulatory subunits in nociceptive neurons. We then tested whether phosphorylation of RII subunits constitutes an endogenous read out for changes in PKA-II activity *in vivo*. By stimulating the neurons with various sensitizing inflammatory mediators we aimed to characterize neuronal subgroups responding to pain-sensitizing stimuli by the expression of nociceptive markers. Our data from fully quantitative and automated high content screening (HCS) microscopy suggest RIIβ can be used as a marker for nociceptive neurons. Moreover, we propose a new dynamic model of baseline RII phosphorylation and its relation to the activity of PKA catalytic subunits.

RESULTS

All PKA regulatory subunits are expressed in DRG neurons

We analyzed the expression of the regulatory (RIα, RIβ, RIIα, RIIβ) and the catalytic (Cα and Cβ) subunits of PKA by real-time PCR. Transcripts of all subunits were detected in mRNA samples of lumbar rat dorsal root ganglions (DRGs; Fig. 1A).

To analyze the expression of the respective PKA subunit proteins, we tested antibodies for their specificity in HeLa cells transiently overexpressing GFP-tagged PKA subunits. All antibodies recognized their respective targets in immunoblots (Fig. 1B). We observed slight cross reactivity of the RIβ antibody to denatured RIα–GFP. Antibodies against the RII subunits, however, proved to be highly specific. In immunostainings of native GFP-tagged PKA regulatory subunits in intact HeLa cells, they showed no sign of cross-reactivity (Fig. 1C) corroborating tests of the RIIβ antibody on tissues of *Pkar2b* knockout mice (Inan et al., 2006). Using these evaluated antibodies, we detected all PKA regulatory subunits in lysates of rat DRGs by immunoblotting (Fig. 1D).

To evaluate the expression of endogenous PKA subunits in DRG neurons at the single cell level, we established a quantitative HCS microscopy approach suitable for the analysis of large numbers of neurons. In brief, the microscope automatically acquires images of immunostained cultures in multi-well plates in up to four fluorescence channels. Neurons are identified by automated image analysis according to their expression of ubiquitin carboxyl-terminal hydrolase L1 (UCHL1, also known as PGP9.5) in combination with object selection parameters optimized for the sphere-like geometry of neurons after short-term culture (Fig. 1E; see Materials and Methods section). Lumbar DRGs (L1–L6) yielded 31,288±3231 analyzable neurons per rat with a unimodal UCHL1 and cell size distribution (Fig. 1F,G).

Using this HCS approach and the evaluated antibodies, we quantified the expression levels of PKA subunits in neurons and non-neuronal cells. In line with findings indicating that the expression pattern of β-isoforms is more restricted (Cadd and McKnight, 1989), we detected β-isoforms only in neurons, whereas α-subunits were expressed also in non-neuronal cells. Cα/β, RIα, RIβ and RIIα were found in all sensory neurons (Fig. 1H). In contrast, RIIβ was restricted to a subpopulation of neurons. Similar staining patterns were present in frozen DRG sections (Fig. 1I).

RIIβ is predominantly expressed in nociceptive neurons

RIIβ was expressed in 68±0.6% (n=4, mean ± s.e.m., total of 44110 neurons) of all cultured DRG neurons and 58±0.9% of all neurons in sections (n=4, mean ± s.e.m., 12,706 neurons; Fig. 2A). Nociceptive C- and Aδ-neurons constitute about 60–70% of DRG neurons and are smaller than other DRG neurons. Indeed, the RIIβ-positive [RIIβ(+)] subpopulation was significantly smaller than the overall neuronal population in cultures (827±6 μm^2 versus 887±7 μm^2, P=0.0005; n=4, mean ± s.e.m., 44,110 neurons) and sections (401±3 μm^2 versus 455±7 μm^2, P=0.006; n=4, mean ± s.e.m., 12706 neurons; Fig. 2B).

Sensory neurons are commonly grouped according the expression of nociceptive subgroup markers such as TRPV1, NaV1.8, calcitonin gene-related peptide (CGRP) and isolectin B4 (IB4), as well as of non-nociceptive markers such as neurofilament 200 (NF200) (Belmonte and Viana, 2008). Using threshold-based quantification, we found 35% of neurons were TRPV1(+), 45% NaV1.8(+), 30% CGRP(+), 51% IB4(+) and 20% NF200(+) in overnight cultures (8000–10,000 neurons; Fig. 2D) and 38% were TRPV1(+), 37% NaV1.8(+), 26% CGRP(+), 40% IB4(+) and 37% NF200(+) in sections (1365–4417 neurons, Fig. 2C,E). In line with previous reports NF200 was mainly detected in large-diameter neurons whereas the nociceptive markers were expressed in smaller neurons (Fig. 2B).

Testing for co-expression with RIIβ, 94% of TRPV1(+), 95% of NaV1.8(+), 90% of CGRP(+) and 80% of IB4(+) neurons also expressed RIIβ in cultured neurons (Fig. 2D). Similarly, in sections 95% of TRPV1(+), 88% of NaV1.8(+), 92% of CGRP(+) and 82% of IB4(+) neurons co-expressed RIIβ (Fig. 2E). In contrast, only 40% and 30% of NF200(+) neurons co-expressed RIIβ in cultures and sections, respectively. Large NF200(+) neurons are known to be Aβ-fibers involved in proprioception but not in nociception. They did not express RIIβ (Fig. 2D,E). Smaller neurons co-expressing RIIβ and NF200 (≈10%) could be moderately myelinated Aδ-fibers involved in the fast detection of first pain (Basbaum et al., 2009). Therefore, RIIβ expression predominates in smaller neurons, including most neurons defined by classical nociceptive markers.

Capsaicin-induced calcium influx occurs predominantly in RIIβ(+) neurons

To corroborate that RIIβ is enriched in nociceptors, we required functional confirmation. We therefore combined Fura-2-based calcium imaging and immunofluorescence analysis using our HCS platform. We stimulated DRG neurons with the pain-inducing TRPV1 ligand capsaicin (250 nM), monitored the calcium influx, and subsequently stained the same fixed cells for RIIβ expression (Fig. 2F). Capsaicin induced calcium influx in 35±5% of all neurons (n=3, total of 942 neurons). In line with immunofluorescence data, 90±0.3% of the capsaicin-responsive neurons were RIIβ(+). Moreover, the mean response amplitude was strongly increased in RIIβ(+) neurons (Fig. 2G).

Raising cAMP levels increases phosphorylation of RII in sensory neurons

Recent data (Manni et al., 2008; Martin et al., 2007; Zhang et al., 2012) suggests that RII subunits should be fully phosphorylated

Journal of Cell Science (2014) 127, 216–229 doi:10.1242/jcs.136580

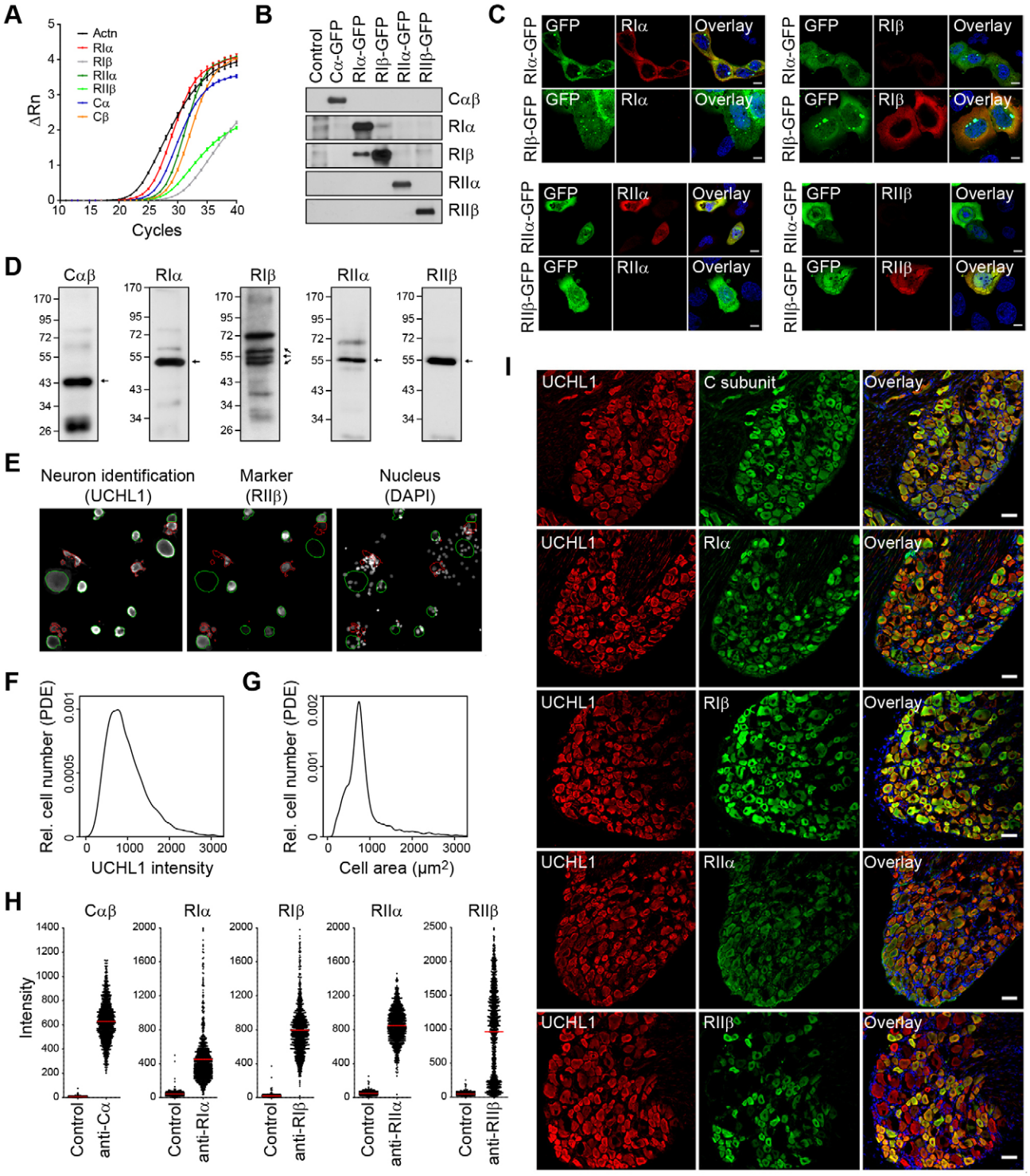

Fig. 1. All main PKA subunits are expressed in DRG neurons. (A) Real-time PCR analysis of the expression of PKA subunits in L1–L6 DRGs at the transcript level. (B) Immunoblots showing GFP-tagged PKA subunits in lysates of transfected HeLa cells. All antibodies recognized their target proteins although slight cross-reactivity of the RIβ antibody with RIα–GFP was observed. (C) Confocal images of immunostained HeLa cells expressing GFP-tagged human PKA subunits with no sign of cross-reactivity. Scale bar: 10 μm. (D) Immunoblots showing the expression of endogenous PKA subunits in whole DRG lysates. All regulatory as well as the catalytic subunits were detected. (E) Representative fields of view showing the image analysis of stained DRG neurons. Green-encircled neurons meet the specified object selection parameters, whereas red-encircled objects not. (F) Distribution of UCHL1 expression in DRG neurons (n=3, 9.6×10^4 neurons). PDE, probability density estimation. (G) Cell size distribution of neurons analyzed in F. (H) Quantitative analysis of stained DRG neurons after overnight culture. All DRG neurons expressed Cα/β, RIα, RIβ and RIIα, whereas RIIβ expression was restricted to a subpopulation (n=1000 neurons per plot). The primary antibody was omitted in the controls. (I) Confocal images of immunostained frozen lumbar DRG sections (10 μm thick; scale bar: 50 μm) verifying the expression pattern in cultures.

Journal of Cell Science (2014) 127, 216–229 doi:10.1242/jcs.136580

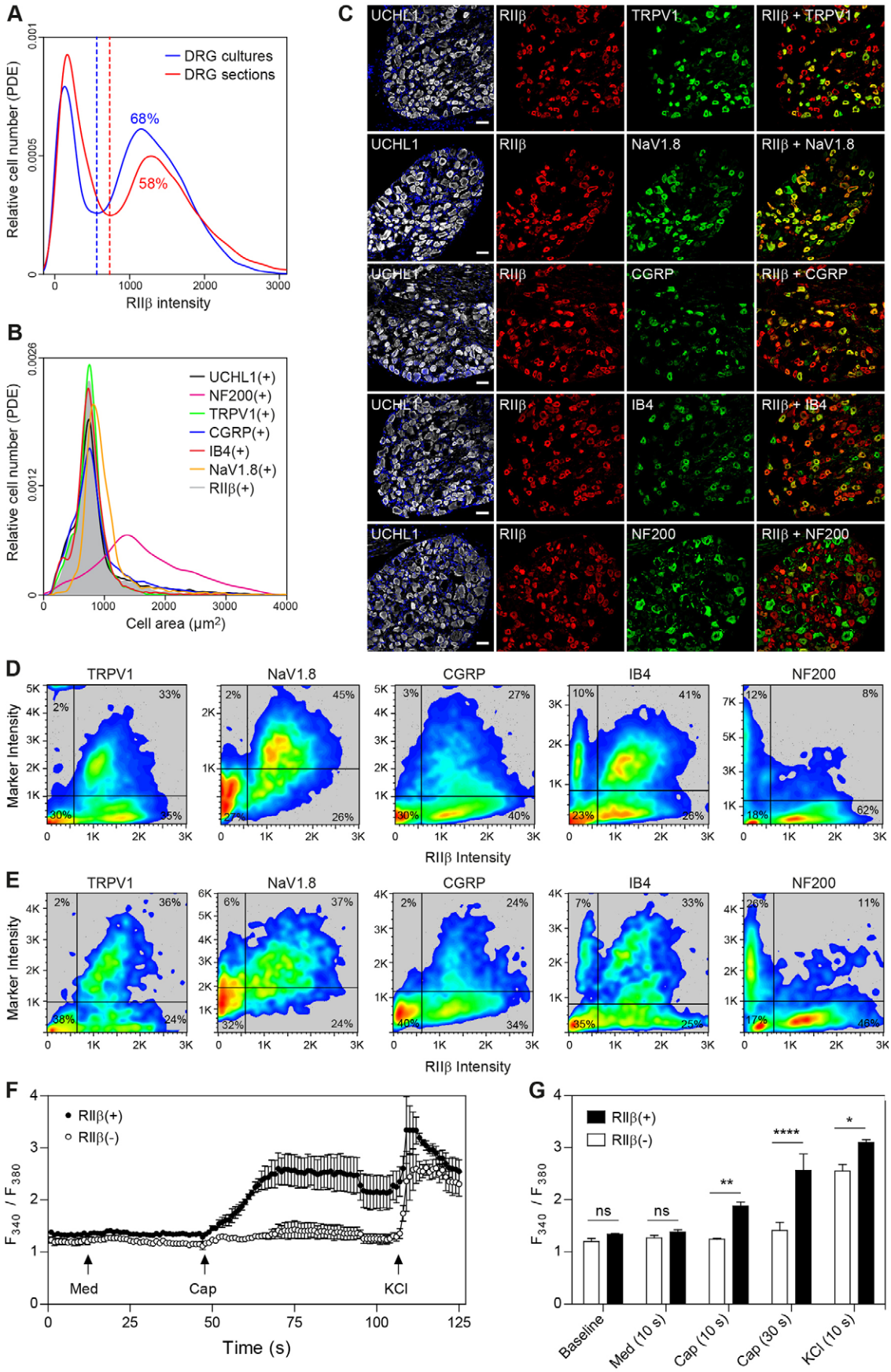

Fig. 2. See next page for legend.

Journal of Cell Science (2014) 127, 216–229 doi:10.1242/jcs.136580

Fig. 2. RIIβ(+) neurons co-express nociceptive markers and respond to capsaicin. (A) Distribution of RIIβ expression in cultured DRG neurons and frozen DRG sections detected by immunostaining. RIIβ expression was restricted to a subpopulation of neurons, 68±0.5% in culture and 58±0.5% in sections. Dashed lines indicate gating thresholds set at local minima to discriminate between RIIβ(−) and RIIβ(+) neurons. PDE, probability density estimation. (B) Size distribution of RIIβ(+) DRG neurons compared with those expressing UCHL1, TRPV1, NaV1.8, CGRP, IB4 or NF200. (C) Confocal images of lumbar DRG sections triple-stained for UCHL1, RIIβ and additional markers (10 μm thick; scale bar: 50 μm). The RIIβ(+) subpopulation included most TRPV1(+), NaV1.8(+), CGRP(+) and IB(+) neurons, but lacked larger NF200(+) neurons. (D) Density plots showing single cell data of cultured DRG neurons labeled for RIIβ and markers TRPV1, NaV1.8, CGRP, IB4 and NF200 (>8000 neurons/plot). Black lines indicate gating thresholds to discriminate between subpopulations. (E) Density plots showing single cell data of DRG neurons in sections labeled for RIIβ and markers [see C, total of 1365 (TRPV1), 2738 (NaV1.8), 4417 (CGRP), 3075 (IB4), 3853 (NF200) neurons]. (F) Mean calcium traces after stimulation with medium (Med), capsaicin (Cap, 250 nM), and potassium chloride (KCl, 30 mM). (G) Statistical analysis of the traces shown in F at baseline, 10 seconds after medium, 10 and 30 seconds after capsaicin, and 10 seconds after KCl stimulation [$n=3$, total of 647 RIIβ(+) and 295 RIIβ(−) neurons, two-way ANOVA with Bonferroni test]. Values are means ± s.e.m. *$P<0.05$; **$P<0.01$; ****$P<0.0001$.

in the inactive PKA-II complex and dephosphorylated after dissociation of the holoenzyme. To test this model in primary sensory neurons, we first verified the specificity of monoclonal antibodies generated against the phosphorylated epitopes of RIIα (rabbit anti-pRII) or RIIβ (mouse anti-pRII). Both antibodies were specific for the phosphorylated epitopes of *in vitro* phosphorylated recombinant RII subunits without discriminating between RIIα and RIIβ (Fig. 3A). Immunoblotting of DRG lysates resulted in double bands of the expected molecular masses (Fig. 3B). In frozen DRG sections, both pRII antibodies produced highly similar staining patterns at the cellular level, although there was nuclear immunoreactivity with the mouse anti-pRII, which was not detected with the rabbit anti-pRII antibody (Fig. 3C).

We then stimulated sensory neurons with the adenylyl cyclase activator forskolin expecting a decrease in pRII signals. To our surprise, forskolin did not decrease, but strongly increased, the pRII signals (Fig. 3D). Signal intensities of both pRII antibodies correlated significantly (Spearman's ρ>0.9; Fig. 3E). Because the dynamic range was higher for the rabbit pRII antibody, we used this antibody for all following experiments.

We performed dose–response and kinetic experiments pharmacologically raising the cellular cAMP concentration. Stimulation with forskolin for 4 minutes increased pRII levels 2.3-fold with a half-maximal effective concentration (EC_{50}) of 1.7 μM (Fig. 4A). Also the membrane-permeable and phosphodiesterase-resistant cAMP analog Sp-8-Br-cAMPS-AM dose-dependently induced RII phosphorylation (EC_{50}=1.3 μM).

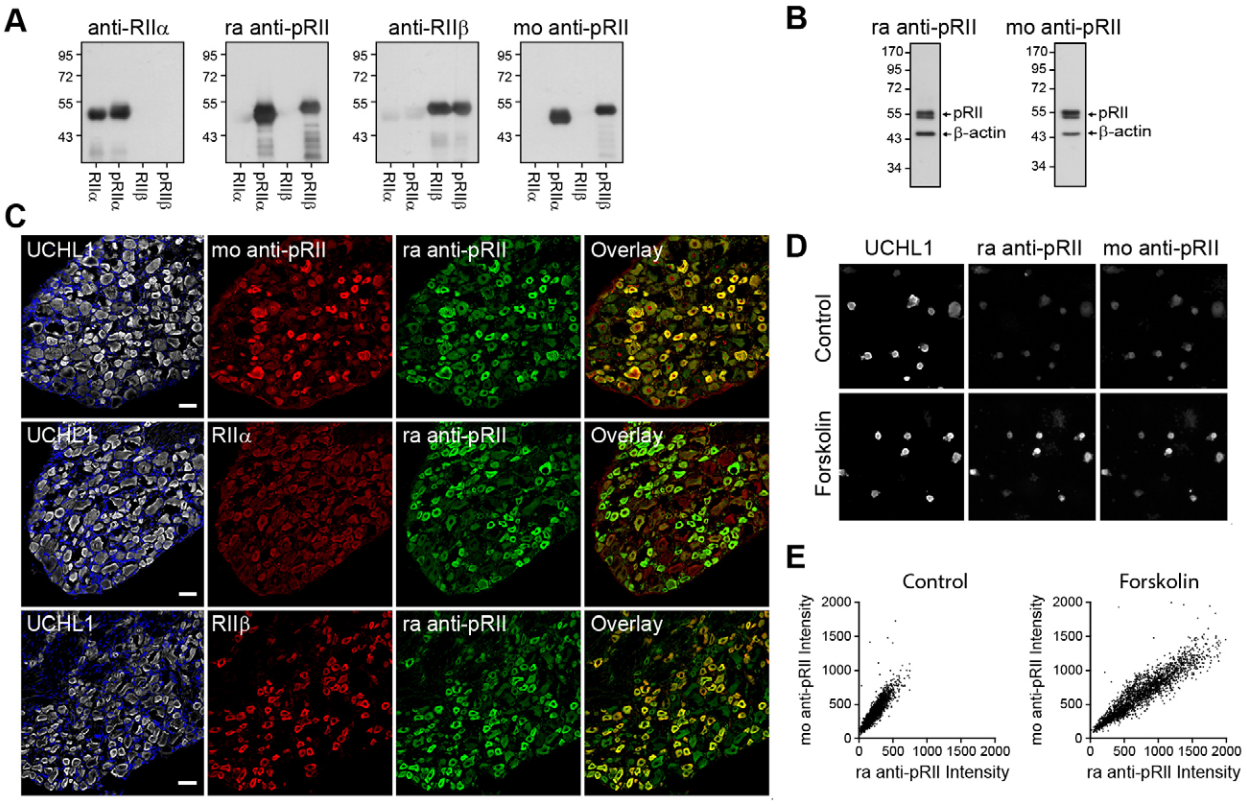

Fig. 3. PKA-mediated phosphorylation of RII subunits represents a measure of PKA-II activity. (A) Immunoblots of *in vitro* phosphorylated RII subunits showing that mouse (mo) and rabbit (ra) pRII antibodies were specific for the phospho-epitopes without discriminating between RII isoforms. (B) Immunoblots of rat DRG lysates probed with mouse or rabbit pRII antibodies. Both antibodies gave rise to double bands at 53 kDa indicating specificity for RII subunits. (C) Confocal images of frozen DRG sections stained for UCHL1, RIIα/β and pRII. The staining pattern of both pRII antibodies was similar and resembled the combined pattern of RIIα/β. (D) Stained DRG cultures after stimulation for 4 minutes with forskolin (10 μM) or solvent control (0.1% DMSO). Forskolin stimulation increased pRII signal intensities. (E) Quantitative immunofluorescence analysis of forskolin (10 μM) and control (0.1% DMSO)-treated DRG neurons. Signal intensities of both pRII antibodies correlated significantly (n>2000 neurons/condition, Spearman's ρ>0.9).

Journal of Cell Science (2014) 127, 216–229 doi:10.1242/jcs.136580

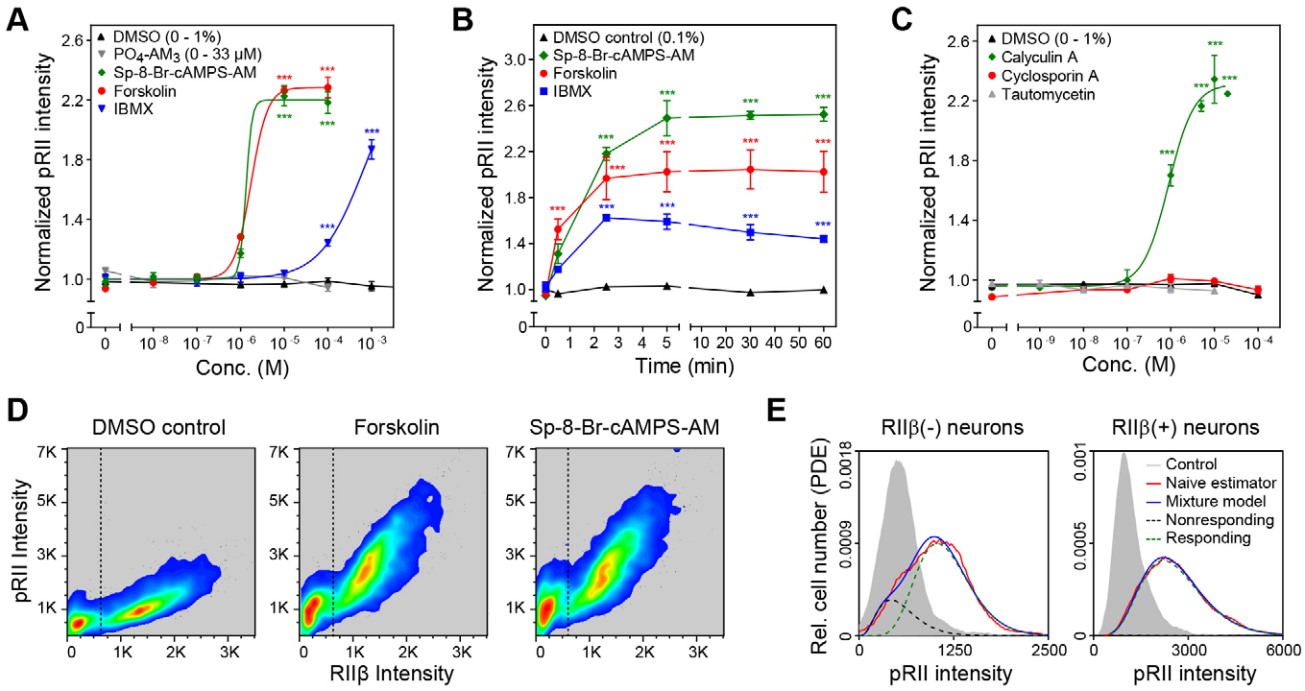

Fig. 4. Pharmacological modulators of cAMP cause long-lasting RII phosphorylation opposed by PP2A-mediated dephosphorylation. (A) Dose–response curves of forskolin (EC_{50}=1.7 µM), Sp-8-Br-cAMPS-AM (EC_{50}=1.3 µM) and IBMX after 4 minutes stimulation (n=3, >2000 neurons/condition; one-way ANOVA with Tukey's test). (B) Time-course experiment indicating long-lasting RII phosphorylation by forskolin (10 µM), Sp-8-Br-cAMPS-AM (10 µM) and IBMX (100 µM). (C) Dose-dependent induction of pRII by calyculin A (EC_{50}=1.7 µM), but not cyclosporine A or tautomycetin after stimulation for 4 minutes. (D) Cell density plots showing pRII/RIIβ-labeled DRG neurons stimulated with forskolin (10 µM), Sp-8-Br-cAMPS-AM (10 µM), or treated with 0.1% DMSO (control; >4000 neurons/condition). Dashed lines indicate gating thresholds to discriminate between RIIβ(−) and RIIβ(+) neurons. (E) Distribution of pRII intensities in RIIβ(−) and RIIβ(+) neurons treated with forskolin (10 µM, red line) compared with the solvent control (0.1% DMSO, gray filled area). Threshold-free mixture modeling (see Materials and Methods section) was applied to estimate the number of non-responsive (dashed black line) and responsive cells (dashed green line) from the modeled population (blue line). PDE, probability density estimation. Values are means ± s.e.m. *P<0.05; **P<0.01; ***P<0.001.

Blocking phosphodiesterases with 3-isobutyl-1-methylxanthine (IBMX) to inhibit cAMP degradation also increased RII phosphorylation (Fig. 4A). The kinetic response to these compounds was long-lasting, reaching plateau values after 5 minutes (Fig. 4B).

The homeostatic level of phospho-RII depends on PP2A

The model of Zhang et al. suggests an immediate phosphorylation of RII subunits even if PKA-II is in a holoenzyme complex (Zhang et al., 2012). Our data, however, show that activation of PKA-II results in a further increase of pRII levels. This suggests that the baseline homeostatic level of phosphorylated RII subunits is controlled by an interplay of catalytic subunits and phosphatases such as calcineurin (PP2B) (Oliveria et al., 2007; Rangel-Aldao and Rosen, 1976) or PP2A (Manni et al., 2008).

We tested whether inhibition of phosphatases PP1, PP2A or calcineurin results in increased homeostatic baseline pRII levels. Treatment with the PP1/PP2A inhibitor calyculin A for 4 minutes resulted in a dose-dependent increase of pRII levels with an EC_{50} of 1.7 µM (Fig. 4C). Treatment with the PP1 inhibitor tautomycetin or the calcineurin inhibitor cyclosporine A did not result in accumulation of phosphorylated RII subunits (Fig. 4C).

The homeostatic level of phospho-RII is increased in RIIβ(+) neurons

Next we compared the basal phosphorylation levels of RIIβ-negative [RIIβ(−)] and RIIβ(+) neurons at the single cell level. RIIβ(+) neurons showed higher pRII levels than RIIβ(−) neurons even in the unstimulated condition (2.5±0.1-fold; n=3, 17,191 neurons; Fig. 4D). This difference was maintained after stimulation with forskolin [2.1±0.1-fold in RIIβ(−) versus 2.3±0.2-fold in RIIβ(+); n=3, 17,715 neurons] indicating that homeostatic pRII levels are regulated in a subgroup-specific manner.

Inflammatory mediators induce transient RII phosphorylation in subpopulations of sensory neurons

We applied a customized mixture modeling approach for the analysis of RIIβ(−) and RIIβ(+) neurons. The method provides the population-based estimate of responding versus non-responding neurons in a threshold-free manner even if populations are largely overlapping (see the Materials and Methods section for details). Forskolin induced RII phosphorylation in 81.8±2.7% of RIIβ(−) and 99.5±0.2% of RIIβ(+) neurons (n=3, 17,715 neurons) indicating that most neurons have the potential to react to increased levels of cAMP (Fig. 4E).

Next we tested whether PKA-II is downstream of known sensitizing inflammatory mediators activating $G\alpha_s$-coupled GPCRs. Stimulation with prostaglandin E_2 (PGE_2) for 30 seconds resulted in a dose-dependent RII phosphorylation with an EC_{50} of 46 nM (Fig. 5A). Prostacyclin (PGI_2, EC_{50}=74 nM) induced a twice as strong response as PGE_2 (Fig. 5A). Testing of several monoamines including serotonin (5-HT), histamine, dopamine, and the β-adrenergic agonist isoproterenol (Iso) revealed that only 5-HT and Iso, but not histamine and dopamine, significantly induced RII

Journal of Cell Science (2014) 127, 216–229 doi:10.1242/jcs.136580

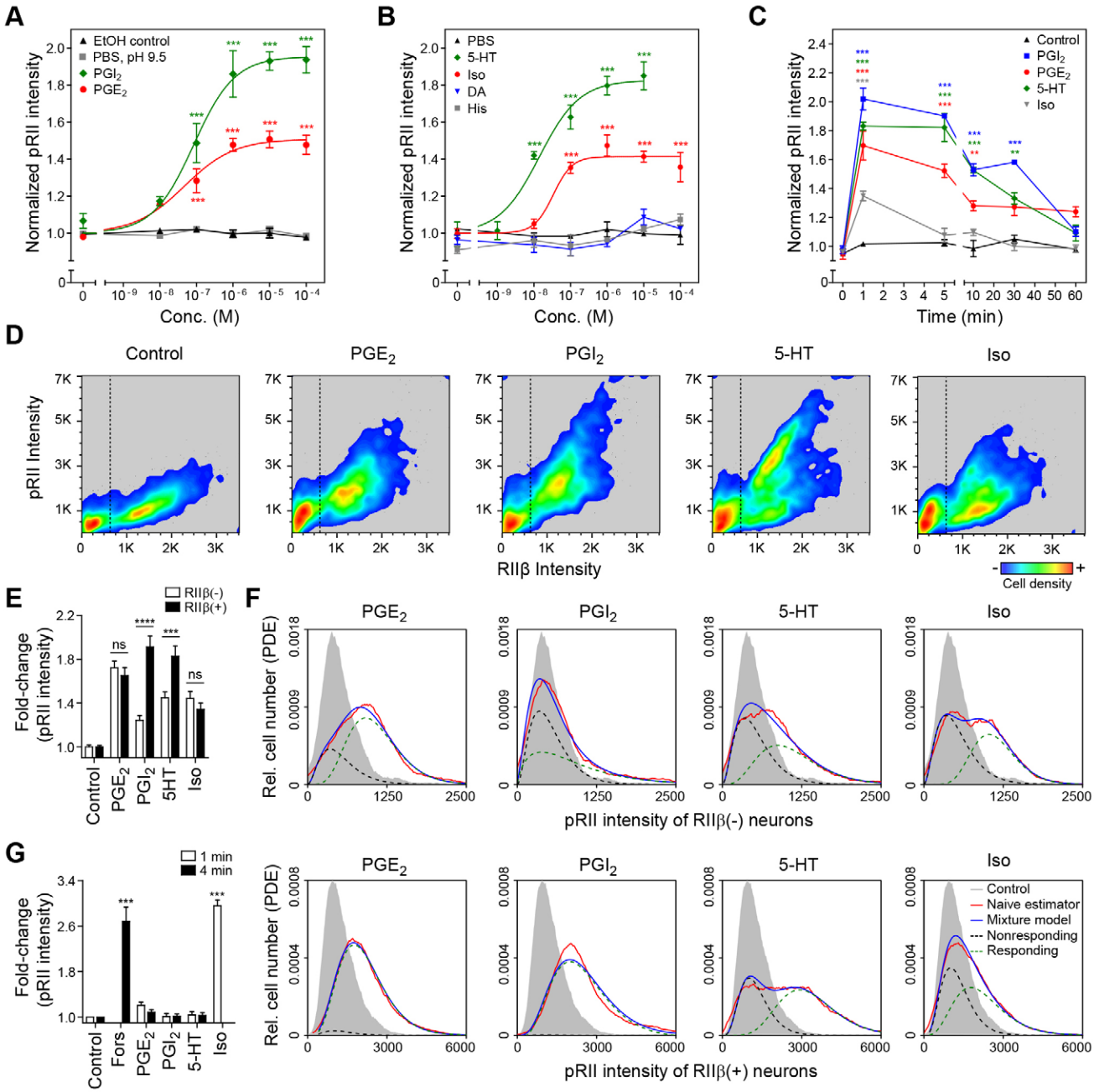

Fig. 5. Inflammatory mediators induce transient RII phosphorylation in different subpopulations of sensory neurons. (A) Dose-dependent induction of pRII after stimulation for 30 seconds with PGE_2 (EC_{50}=46 nM) and PGI_2 (EC_{50}=74 nM) (n=3, >2000 neurons/condition; one-way ANOVA with Tukey's test). (B) Dose–response curves of serotonin (5-HT, EC_{50}=14 nM) and isoproterenol (Iso, EC_{50}=33 nM) after 30 seconds stimulation. Related monoamines dopamine (DA) and histamine (His) did not change pRII levels. (C) Time-course experiment showing transient RII phosphorylation by PGE_2 (10 μM), PGI_2 (10 μM), 5-HT (1 μM) and Iso (1 μM). (D) Density plots showing pRII/RIIβ-labeled DRG neurons stimulated for 1 minute with PGE_2 (10 μM), PGI_2 (10 μM), 5-HT (1 μM) or Iso (1 μM) (>4000 neurons/condition). Dashed lines indicate gating thresholds to discriminate between RIIβ(−) and RIIβ(+) neurons. (E) Fold changes of pRII intensities in RIIβ(−) (white bars) and RIIβ(+) (black bars) neurons after stimulation for 1 minute (n=3, >2000 neurons/condition, two-way ANOVA with Bonferroni test). (F) Distribution of pRII intensities from stimulated (red lines) and solvent control-treated (gray filled areas) RIIβ(−) (upper panel) and RIIβ(+) (lower panel) DRG neurons shown in D. Mixture modeling (see Materials and Methods section) was applied to estimate the number of non-responsive (dashed black line) and responsive cells (dashed green line) from the modeled population (blue line). Notably, RIIβ(+) neurons selectively react to PGI_2. (G) Average pRII levels in non-neuronal cells after stimulation (n=3, >2000 neurons/condition; one-way ANOVA with Tukey's test). Values are means ± s.e.m. *P<0.05; **P<0.01; ***P<0.001.

phosphorylation (Fig. 5B). The EC_{50} values were 14 nM for 5-HT and 33 nM for Iso, respectively. In contrast to the effects of cAMP analogs, PKA-II activation induced by inflammatory mediators was transient. Maximal responses were reached within 1 minute, returning to baseline within 5 to 60 minutes (Fig. 5C).

In order to analyze the response to each inflammatory mediator at the single cell level, we stimulated DRG neurons for 1 and 4 minutes and immunostained for pRII and RIIβ (Fig. 5D). PGE_2 broadly activated RIIβ(+) as well as RIIβ(−) neurons, whereas responses to PGI_2, 5-HT, and Iso were restricted to

Journal of Cell Science (2014) 127, 216–229 doi:10.1242/jcs.136580

subpopulations. Notably, PGI_2- and 5-HT-induced RII phosphorylation was significantly higher in RIIβ(+) neurons (Fig. 5E).

To show that raising cAMP levels also induces RII phosphorylation in non-neuronal cells such as glia, we quantified pRII levels in non-neuronal cells using a modified cell identification algorithm, which selects smaller sized, bright nuclei of cells lacking expression of UCHL1. We found that only forskolin and Iso, but not PGI_2 and 5-HT, significantly increased pRII levels in non-neuronal cells (Fig. 5G).

We used our mixture modeling approach to quantify the percentage of responsive neurons and found strong differences between the inflammatory mediators with respect to the activated subpopulations. PGE_2 induced RII phosphorylation in 69±5% of RIIβ(−) and 92±5% of RIIβ(+) neurons after 1 minute stimulation (Fig. 5F, n=3, 10,464 neurons). Similar results were obtained after 4 minutes stimulation [67±3% of RIIβ(−) and 82±10% of RIIβ(+) neurons, n=3, 16,933 neurons]. Of note, PGI_2 was selectively acting on RIIβ(+) neurons after 1 minute (99±0.4%, n=3, 10,505 neurons) and 4 minutes stimulation (99±0.6%, n=3, 10,555 neurons), but had no significant effect on RIIβ(−) neurons. 5-HT stimulation caused RII phosphorylation in subpopulations of RIIβ(−) and RIIβ(+) neurons after 1 minute [49±5% of RIIβ(−) and 62±2% of RIIβ(+) neurons, n=3, 9470 neurons] and 4 minutes [58±1% of RIIβ(−) and 63±1% of RIIβ(+) neurons, n=3, 16,352 neurons]. Iso induced RII phosphorylation in both neuron populations after 1 minute stimulation [43±3% of RIIβ(−) and 56±3% of RIIβ(+) neurons, n=3, 9808 neurons].

Thus, changes in pRII levels allow subgroup-specific analysis identifying that some inflammatory mediators activate PKA-II in most neurons (e.g. PGE_2) and others specifically act on subgroups (e.g. PGI_2, 5-HT).

PGI_2- and 5-HT-induced RII phosphorylation is followed by PKA-dependent CREB phosphorylation

The expression of RIIβ and the dynamic phosphorylation of RII allowed us to analyze the kinetics of ligand-induced signaling in a subgroup-specific manner. It remained unclear, however, if phosphorylation of RII subunits indicates increased activity of PKA-II catalytic subunits. We therefore tested whether the increase of pRII is followed by increased phosphorylation of a PKA downstream target such as the transcription factor CREB. CREB is phosphorylated at Ser133 within its kinase-inducible domain by several kinases including PKA and ERK1/2.

Stimulation with forskolin induced nuclear CREB phosphorylation in DRG neurons detected with a phospho-Ser133-specific antibody (Fig. 6A). Quantification of signal intensities from time course experiments revealed a long-lasting response upon forskolin stimulation (Fig. 6B). Inflammatory mediators by contrast induced transient CREB phosphorylation, peaking 5 minutes after stimulation (Fig. 6B). In agreement with CREB being a downstream target of PKA, the response kinetics were slightly slower than the pRII response (Fig. 5C).

For an estimate of the number of responding cells, we analyzed pCREB/RIIβ-labeled neurons stimulated for 4 minutes (Fig. 6C). Basal pCREB levels were 1.3±0.01-fold higher in RIIβ(+) compared with RIIβ(−) neurons (n=3, 11,268 neurons), probably reflecting the higher basal PKA-II activity in RIIβ(+) neurons shown above. In line with the pRII-based subgroup analysis, we found that forskolin and PGE_2 induced CREB phosphorylation in both populations to a similar extent, whereas responses to PGI_2 and 5-HT were significantly higher in RIIβ(+) neurons (Fig. 6D).

Applying mixture modeling revealed that forskolin stimulation induced CREB phosphorylation in most neurons [70±1% of RIIβ(−) and 88±2% of RIIβ(+) neurons, n=3, 10,407 neurons; Fig. 6E]. PGE_2 induced a broad and rather weak response in both populations [54±3% of RIIβ(−) and 74±7% of RIIβ(+) neurons, n=3, 11,392 neurons]. PGI_2-induced CREB phosphorylation was restricted to RIIβ(+) neurons (79±3%, n=3, 11,641 neurons). 5-HT acted on both populations, but the response was enhanced in RIIβ(+) neurons [38±6% of RIIβ(−) and 65±6% of RIIβ(+) neurons, n=3, 10,797 neurons].

To analyze whether CREB phosphorylation was dependent on PKA but not ERK1/2, we pretreated the neurons for 1 hour with the PKA inhibitor H89 or with the MEK inhibitor PD98059. CREB phosphorylation was blocked by the inhibitor of PKA but not of MEK (Fig. 6F). To verify the effectiveness of PD98059, ERK1/2 phosphorylation induced by the nerve growth factor (1 nM, 30 minutes) was blocked by PD98059 (Fig. 7A). Therefore, induction of RII phosphorylation indicates that there is activation of PKA-II as confirmed by PKA-dependent phosphorylation of its downstream target, CREB.

PGE_2 selectively activates PKA-II in DRG-derived F11 cells

Our pRII assay specifically detects the activation of PKA-II but not of PKA-I. In order to test all PKA isoforms for activation by inflammatory mediators, we employed bioluminescence resonance energy transfer (BRET) sensors. These are composed of *Renilla* luciferase-conjugated R-subunits (hRIα-RLuc, hRIIα-RLuc and hRIIβ-RLuc) as bioluminescent donor proteins and GFP-tagged catalytic subunits as acceptor proteins (Diskar et al., 2007; Prinz et al., 2006a; Prinz et al., 2006b). In the inactive PKA complex the close proximity of luciferase and GFP results in energy transfer and a strong BRET signal. Activation of PKA by cAMP results in dissociation of the subunits reducing BRET signals.

Because BRET requires recombinant expression of fusion proteins, we switched to DRG-derived F11 cells. Forskolin strongly activated PKA-Iα, PKA-IIα and PKA-IIβ sensors as indicated by the drop of the BRET signal to 71±10%, 30±7% and 22±4%, respectively (Fig. 7B–D). The inflammatory mediator PGE_2 also activated PKA. In contrast to forskolin, PGE_2 selectively activated PKA-IIα (65±6%) and PKA-IIβ sensors (77±9%).

DISCUSSION

Dynamics of PKA-RII phosphorylation

Combinatorial assembly of catalytic and regulatory subunits results in diverse isoforms of the PKA family. Their quaternary structures differ substantially (Taylor et al., 2012). A detailed analysis of isoform-specific cellular functions, however, remains challenging. Approaches to directly detect the activation of endogenous isoforms in primary cells models are largely missing. It was unclear whether changes in RII phosphorylation reflect the process of PKA-II activation. Early biochemical studies on PKA-II purified from bovine cardiac muscle showed that a large proportion of PKA-II is phosphorylated *in vivo* (Rangel-Aldao et al., 1979). Another report suggests that RII subunits are fully phosphorylated in non-stimulated cardiomyocytes (Manni et al., 2008). Accordingly, these researchers found that activation of PKA resulted in a phosphatase-dependent loss of basal RII phosphorylation detected in cell lysates (Manni et al., 2008). The assumption that RII subunits are fully phosphorylated in the inactive holoenzyme complex was also suggested by the recently

Journal of Cell Science (2014) 127, 216–229 doi:10.1242/jcs.136580

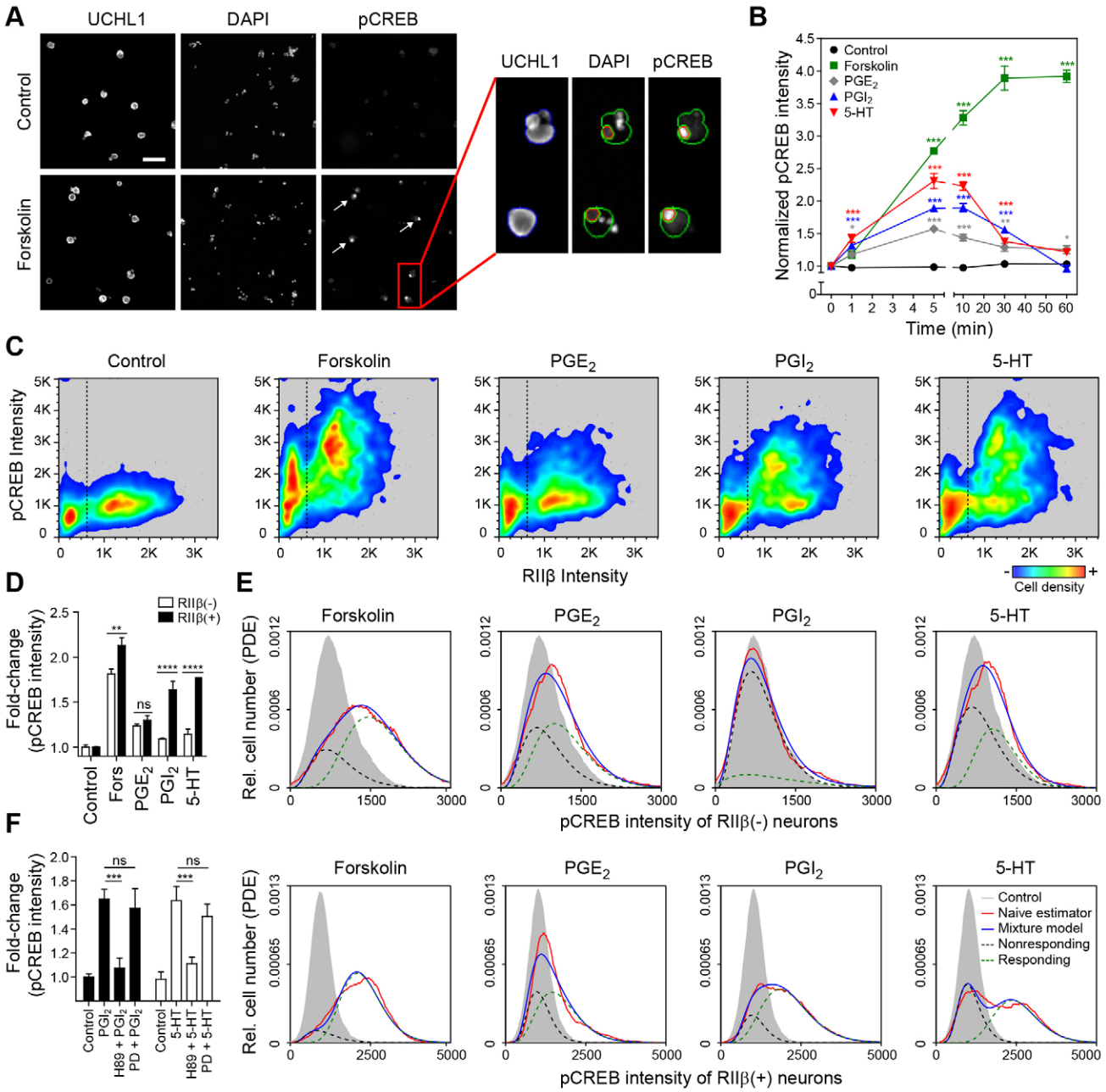

Fig. 6. PGI_2- and 5-HT-induced CREB phosphorylation depends on PKA and occurs predominantly in RIIβ(+) neurons. (A) Immunostaining of phospho-CREB (pCREB) in DRG neurons stimulated for 15 minutes with forskolin (10 μM) or treated with solvent (0.1% DMSO; control). Scale bar: 20 μm. (B) Time course of pCREB by forskolin (10 μM), PGE_2 (10 μM), PGI_2 (10 μM) or 5-HT (1 μM) (n=3, >2000 neurons/condition; one-way ANOVA with Tukey's test). (C) Cell density plots showing pCREB/RIIβ-labeled DRG neurons stimulated for 4 minutes with forskolin (10 μM), PGE_2 (10 μM), PGI_2 (10 μM) or 5-HT (1 μM) (n>4000 neurons per plot). Dashed lines indicate gating thresholds to discriminate between RIIβ(−) and RIIβ(+) neurons. (D) Fold changes of pCREB intensities in RIIβ(−) (white bars) and RIIβ(+) (black bars) neurons after 4 minutes stimulation with forskolin or inflammatory mediators (n=3, >2000 neurons/condition, Two-way ANOVA with Bonferroni test). (E) Distribution of pCREB intensities from stimulated (red lines) and solvent-treated (gray filled areas) RIIβ(−) (upper panel) and RIIβ(+) (lower panel) DRG neurons shown in C. Mixture modeling was applied to estimate the number of non-responsive (dashed black line) and responsive cells (dashed green line) from the modeled population (blue line). (F) Fold changes of pCREB from DRG neurons pretreated for 1 hour with the PKA inhibitor H89 (25 μM) or with the MEK inhibitor PD98059 (50 μM) and then stimulated with PGI_2 (1 μM) or 5-HT (1 μM) for 4 minutes (n=3, >2000 neurons/condition, one-way ANOVA with Tukey's test). CREB phosphorylation was blocked by the PKA, but not the MEK inhibitor. Values are means ± s.e.m. *P<0.05; **P<0.01; ***P<0.001.

resolved crystal structure of the PKA-RIIβ tetrameric holoenzyme ($RII\beta_2$:C_2) (Zhang et al., 2012). Only the reaction products ADP and phosphorylated RIIβ were detected after diffusion of MgATP into the $RII\beta_2$:C_2 crystals in the absence of cAMP (Zhang et al., 2012). Based on these findings, Zhang et al. proposed that the $RII\beta_2$:C_2 holoenzymes are instantly autophosphorylated in the inactive state. Based on this model, cAMP-induced dissociation of the complex would result in dephosphorylation of free pRII by nearby phosphatases (Manni et al., 2008; Oliveria et al., 2007; Zhang et al., 2012).

Journal of Cell Science (2014) 127, 216–229 doi:10.1242/jcs.136580

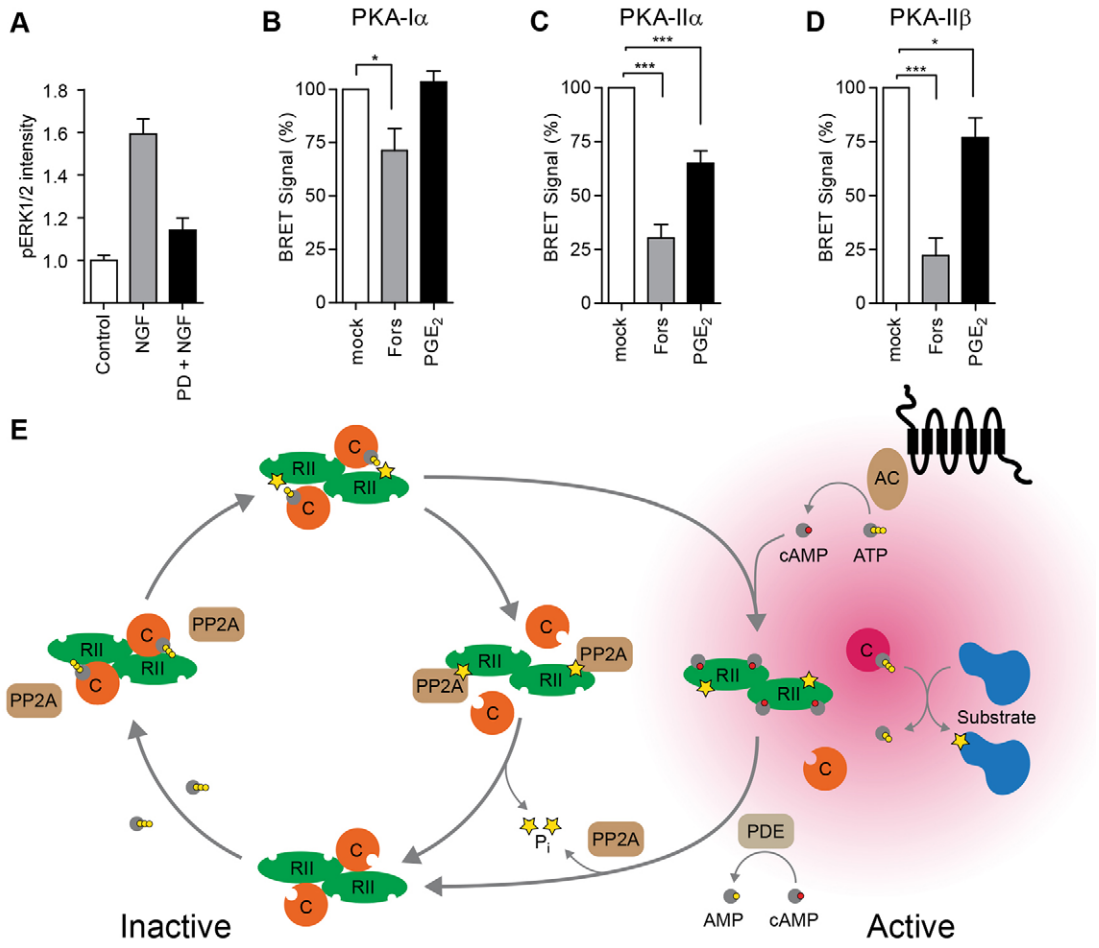

Fig. 7. (A) The MEK inhibitor PD98059 (50 μM) blocks nerve growth factor (NGF)-induced (1 nM, 30 minutes) ERK1/2 phosphorylation. (B–D) PGE_2 selectively activates PKA-II, but not PKA-I, in transiently transfected F11 cells. DRG-derived F11 cells were transfected with isoform-specific BRET sensors composed of GFP-hCα and hRIα-RLuc (B), hRIIα-RLuc (C), or hRIIβ-RLuc (D), 48 hours prior to stimulation with forskolin (10 μM) or PGE_2 (10 μM). Control transfections with fusion proteins only were performed to determine the background (n=3; one-way ANOVA). Values are means ± s.e.m. *P<0.05; **P<0.01; ***P<0.001. (E) Proposed model of PKA-II activation. We extended the model as proposed by Zhang et al. (Zhang et al., 2012). RII subunits are phosphorylated by C-subunits within the tetrameric RII_2C_2 complex resulting in dissociation of the complex. Rapid dephosphorylation by PP2A induces reassociation of the PKA-II complex followed by a new cycle of RII phosphorylation/dephosphorylation. Activation of adenylyl cyclases (AC) results in local production of cAMP, which binds to RII subunits. Binding of cAMP stabilizes RII phosphorylation and leads to the dissociation of the PKA-II complex resulting in release of active C-subunits phosphorylating nearby substrates. Degradation of cAMP by phosphodiesterases (PDEs) is followed by dephosphorylation and reassociation with free C-subunits.

Using a novel HCS microscope approach for the analysis of adult sensory neurons, we found high variability of basal pRII levels. Especially high levels were detected in sensory neurons with high expression levels of RIIβ (Fig. 4D). Interestingly, these neurons coexpress markers of nociceptive neurons, suggesting that they are functionally distinct (Fig. 2C–E). In contrast to the model of PKA-II activation depicted above, raising cAMP levels resulted in increased phosphorylation of endogenous RII subunits in our experiments. The induction of pRII was observed in response to activators of adenylyl cyclases, cAMP analogs, block of cAMP hydrolysis by phosphodiesterases, and ligand induced activation of $G\alpha_s$-coupled GPCRs (Figs 4, 5).

We believe, however, that our data are not contradictory to the recently published data. Rather, our findings extend the current model by further information about the basal state. Instant phosphorylation of RII, as suggested by Zhang et al. (Zhang et al., 2012), could be counterbalanced *in vivo* by rapid dephosphorylation even in the absence of cAMP (Fig. 7E). Indeed, blocking the phosphatase PP2A in the absence of any stimulatory signal resulted in increased basal pRII signals (Fig. 4C). This model is supported by the observed decrease of the K_d for the interaction of RII with C-subunits following RII phosphorylation by factor of five (Rangel-Aldao and Rosen, 1976; Zimmermann et al., 1999). Also studies using BRET sensors demonstrate that phosphorylation of RII subunits is required for the full dissociation of PKA-II holoenzymes in cell lines (Diskar et al., 2007). Thus, we propose to extend the current model as follows: (I) RII subunits are instantly phosphorylated by C-subunits within the tetrameric RII_2C_2 complex; (II) pRII has a higher probability for brief dissociation of the tetrameric complex; (III) free pRII subunits are rapidly dephosphorylated by PP2A and/or calcineurin, which induces reassociation of the complex followed by a new cycle of RII phosphorylation and dephosphorylation (Fig. 7E).

The introduction of rapid turn-over at pRII in the basal state has important implications. Our data indicate that

Journal of Cell Science (2014) 127, 216–229 doi:10.1242/jcs.136580

measuring endogenous pRII levels allows the isoform-specific analysis of endogenous PKA-II activation even in hard to transfect cells such as the adult nociceptive neurons. The kinetics of RII phosphorylation measured here closely resemble the kinetics observed using the FRET-based sensor AKAR2 that monitors the activity of C-subunits (Zhang et al., 2005). Furthermore, changes at the level of pRII resemble substrate phosphorylation because the response strength, kinetics and number of responding cells is similar for RII and CREB phosphorylation (Figs 5, 6). Also the dissociation constants from dose–response experiments are consistent with previous reports derived from reporter-based methods (Prinz et al., 2006a). In line with our findings, increased RII phosphorylation was recently detected in spinal cord neurons following intrathecal injection of NMDA (Kim et al., 2011). As we found pRII responses in glia cells, this also applies to non-neuronal cell types (Fig. 5G). We conclude that pRII antibodies can be used to analyze the isoenzyme-specific activation of endogenous PKA-II.

The investigation of the dynamics of RII phosphorylation revealed surprising aspects. Phosphorylation sites of RII are excellent substrates for the phosphatase calcineurin (PP2B), which has also been reported to colocalize with RII at the C-terminus of AKAP79/150 in neurons (Oliveria et al., 2007; Rangel-Aldao and Rosen, 1976). We therefore assumed that dephosphorylation of RII is mediated by calcineurin. However, in nociceptive neurons it is not calcineurin but PP2A that seems to be involved in the regulation of the basal state (Fig. 4C). This observation is in line with findings in cell lysates of forskolin-stimulated cardiac myocytes in which dephosphorylation of RII subunits could also be inhibited by the PP2A inhibitor calyculin A (Manni et al., 2008).

PKA-RIIβ, a subgroup marker predominantly expressed in nociceptive neurons

We set out to investigate subgroup specificity of PKA isoforms. We found RIIβ to be selectively expressed in a subgroup of sensory neurons (≈60%, Fig. 2A). Interestingly, the neurons in this subgroup include most neurons labeled by classical nociceptive markers and they are activated by the pain-eliciting TRPV1 agonist capsaicin (Fig. 2C–G). Our findings therefore reveal that not only specific ion channels, but also signaling components modulating these channels, show subgroup-specific expression patterns and are enriched in nociceptive neurons. This suggests that also the intracellular signaling machinery defines the function of nociceptive subgroups. Currently there is no marker that exclusively identifies nociceptive neurons. As for the classical markers, RIIβ is expressed predominantly in nociceptive neurons and thus may be used equally as a marker of nociceptive neurons. Nevertheless, further studies are required to clarify whether RIIβ expression is restricted to nociceptive subgroups only or to what extend RIIβ expression occurs also in some non-nociceptive subgroups (e.g. itch-specific neurons).

Inflammatory mediators modulate various ion channels including TRPV1, NaV1.8 and P2X3 in nociceptive neurons in a PKA-dependent manner (Bhave et al., 2002; England et al., 1996; Fitzgerald et al., 1999; Moriyama et al., 2005; Rathee et al., 2002; Wang et al., 2007). Sensitization of TRPV1 depends on its association with AKAP79/150 to form a signaling complex that includes PKA (Bhave et al., 2002; Jeske et al., 2008; Rathee et al., 2002; Schnizler et al., 2008; Zhang et al., 2008). This implies that PKA-II isoforms bound to AKAPs are more relevant for sensitization of ion channels in nociceptive neurons. Supporting this, our data demonstrate that the transcription factor CREB is downstream of PKA-II-mediated sensitization signaling and is predominantly activated in RIIβ(+) neurons. This suggests a PKA-II-dependent induction of transcriptional long-term changes such as seen for example during chronification of pain.

We found that PGE_2 selectively activates PKA-II, but not PKA-I (Fig. 7B–D). Also, a study using BRET sensors in COS-7 cells showed that stimulation of β-adrenergic receptors with isoproterenol selectively dissociated RIIα holoenzymes but not RIα holoenzymes (Prinz et al., 2006a). In addition, we found inflammatory mediators to activate PKA-II in RIIβ(+) as well as RIIβ(−) neurons. This suggests that RIIα and RIIβ are activated downstream of $G\alpha_s$-coupled GPCRs in sensory neurons and are functionally redundant. Isoform replacement could therefore explain why knockout mice of individual RII isoforms present rather mild phenotypes (Brandon et al., 1998; Cummings et al., 1996; Rao et al., 2004).

Our pRII assay allowed us to investigate the dynamics of PKA-II in subgroups of sensory neurons. To what extent inflammatory mediators act on sensory neurons has not been analyzed in detail so far. We found some inflammatory mediators to activate PKA-II in nearly all DRG neurons (e.g. PGE_2), whereas others acted on subgroups of RIIβ(−) and RIIβ(+) neurons (e.g. 5-HT, Iso) or even specifically activated RIIβ(+) neurons only (e.g. PGI_2; Fig. 5F). The observation that PGI_2 induces RII and CREB phosphorylation selectively in RIIβ(+) neurons underlines the importance of RIIβ as a possible marker predominantly expressed in nociceptive subgroups. Peripheral sensitization by PGI_2 acting on IP_1 receptors is well described (Pulichino et al., 2006). Mice deficient for the PGI_2 receptor showed reduced inflammation and pain comparable with that of NSAID treatment in models of acute and chronic inflammation (Murata et al., 1997; Pulichino et al., 2006). In contrast to PGE_2, PGI_2-induced sensitization is restricted to the peripheral sensory system and does not occur within the spinal cord (Pulichino et al., 2006; Reinold et al., 2005). This corroborates that RIIβ(+) neurons are enriched for nociceptive neurons and identifies PKA-RIIβ downstream of IP1 receptors as a potential novel therapeutic target in the peripheral nervous system.

The great challenge of signaling analysis is the identification of isoform-specific actions in subgroups of primary cells. The novel HCS microscopy approach presented here enables the investigation of PKA-II dynamics in intact primary sensory neurons. Analyzing more than 1 million neurons, this approach elucidated the dynamic nature of the PKA-II basal state as well as subgroup-specific actions of inflammatory mediators. Beyond the suggestion of a new potential therapeutic target and the extension of the current model of PKA-II activation, our work further proposes a general assay for the analysis of endogenous PKA-II activation in primary cells.

MATERIALS AND METHODS

Animals

Male Sprague Dawley rats (200–225 g, 8 weeks old) were obtained from Harlan. All animal experiments were performed in accordance with the German animal welfare law with permission of the District Government of Berlin (LaGeSo, Berlin, license ZH120). For tissue collection, rats were killed by CO_2 inhalation.

Antibodies

The following antibodies were used: rabbit polyclonal anti-Cα (Santa Cruz, no. sc-903; WB 1:5000, IC 1:500), rabbit monoclonal anti-RIα

(Cell Signaling, no. 5675; WB 1:5000, IC 1:1000), rabbit polyclonal anti-RIβ (Abm, no. Y051648; WB 1:2500, IC 1:500), mouse monoclonal anti-RIIα (BD Transduction Laboratories, no. 612242; WB 1:5000, IC 1:500), mouse monoclonal anti-RIIβ (BD, no. 610625; WB 1:5000, IC 1:2000), mouse monoclonal anti-phospho-RIIβ (S114) (BD, no. 612550; WB 1:2000, IC 1:1000), rabbit monoclonal anti-phospho-RIIα (S96) (Abcam, no. ab32390; WB 1:2000, IC 1:1000), chicken polyclonal anti-UCHL1 (Novus, no. NB110-58872; IC 1:2000), rabbit polyclonal anti-TRPV1 (Alomone, no. ACC-030; IC 1:1000), mouse monoclonal anti-neurofilament 200 labeled with Alexa Fluor 488 (Sigma-Aldrich, no. N0142; IC 1:500), rabbit polyclonal anti-CGRP (Bachem, no. T-4032; IC 1:1000), rabbit polyclonal anti-NaV1.8 (Abcam, no. ab63331; IC 1:500), FITC-conjugated isolectin B4 (Sigma, L2895; IC 1:2500), highly cross-adsorbed Alexa-Fluor-647-, -594 and -488-conjugated secondary antibodies (Invitrogen).

Reagents

Forskolin (no. F3917), 3-isobutyl-1-methylxanthine (IBMX, no. I7018), GR113808 (#G5918), serotonin hydrochloride (5-HT, no. H9523), histamine dihydrochloride (no. H7250), dopamine hydrochloride (no. H8502), (−)-isoproterenol hydrochloride (no. I6504), cyclosporine A, and capsaicin were from Sigma-Aldrich. Phosphate tris(acetoxymethyl)ester (PO_4-AM_3, no. P030-003), 8-bromoadenosine 3′,5′-cyclic monophosphorothioate, Sp-isomer and acetoxymethyl ester (Sp-8-Br-cAMPS-AM, no. B029) were from Biolog LSI. PGE_2 (no. 14010) and PGI_2 (no. 18220) were from Cayman. PD98059 was from Calbiochem. H89 dihydrochloride, calyculin A and tautomycetin were from Tocris. All drugs were prepared as 10–100 mM stocks in distilled water, PBS, DMSO or ethanol.

Real-time PCR

RNA was isolated using Trizol (Invitrogen). One µg total RNA was reverse transcribed using the Multi-Scribe RT kit (Applied Biosystems). Reactions were performed in triplicate using TaqMan probes. FAM-coupled TaqMan probes (Rn00566036, Rn01756450, Rn00709403, Rn01293014, Rn01432302, Rn01748544, Rn00667869) were from Applied Biosystems.

Immunoblotting

L1–L6 DRGs were pulverized in liquid nitrogen and lysed in 1 ml lysis buffer (15 mM Tris-HCl (pH 7.5), 8 M urea, 8.7% glycerol, 1% sodium dodecyl sulfate, 143 mM β-mercaptoethanol). Lysates were homogenized (QIAShredder, Qiagen), denatured for 5 minutes at 95℃, loaded (10 µg), separated by SDS-PAGE, and transferred to PVDF membranes (Millipore). After blocking in Tris-buffered saline (TBST) with 2.5% milk powder at 4℃ overnight, membranes were incubated with the primary antibody diluted in TBST for 3 hours at room temperature (RT). After three washes with TBST (10 minutes, RT), a chemiluminescence detection system was used (Thermo Fisher).

Expression of PKA regulatory subunits in HeLa cells

HeLa cells were seeded on 12 mm coverslips placed in 24-well plates at a density of 2.5×10^4 cells/well and transfected with Lipofectamine 2000 (Invitrogen) on the following day, according to the manufacturer's instructions. C-terminally GFP-tagged R-subunits are described elsewhere (Prinz et al., 2006a). Cells were fixed with paraformaldehyde (PFA, 4%, 10 minutes) after 36 hours and stained as described below.

In vitro phosphorylation of PKA regulatory subunits

Recombinant human RIIα and RIIβ (5 µg) were diluted in 50 µl 20 mM MOPS (pH 7.0), 50 mM NaCl, 10 mM $MgCl_2$ and 1 mM ATP. Samples were mixed, split in half, spiked with either 100 nM PKA-Cα or buffer, and incubated for 30 minutes at RT. Reactions were stopped by adding 5× SDS sample buffer and heating to 95℃ for 10 minutes.

DRG neuron cultures

L1–L6 DRGs were removed, desheathed, pooled and incubated in Neurobasal A medium supplemented with B27 (Invitrogen) and collagenase P (Roche; 0.2 U/ml) for 1 hour at 37℃ in 5% CO_2. The neurons were dissociated by trituration with fire-polished Pasteur pipettes. Axon stumps and disrupted cells were removed by BSA gradient centrifugation (15% BSA, 120 ***g***, 8 minutes). Cells were resuspended in Neurobasal A supplemented with B27 medium, plated on 96-well imaging plates (Greiner) or onto glass coverslips precoated with poly-L-ornithin (0.1 mg/ml) and laminin (5 µg/ml), and incubated overnight (37℃, 5% CO_2). Neuron density was ~1500 neurons/cm^2.

Frozen DRG sections

L1–L6 DRGs were fixed with 2% PFA for 4 hours on ice, rinsed three times for 20 minutes with PBS at RT, submerged in 30% sucrose in PBS at 4℃ overnight, embedded in Tissue Tek (EMS Science), and snap frozen on dry ice. Frozen blocks were cut into 10 µm sections, mounted on slides, dried for 30 minutes at RT, and stored at −80℃. Thawed sections were fixed in 2% PFA for 10 minutes at 4℃, rinsed in PBS for 30 minutes, and stained as described below.

Stimulation of DRG neurons

DRG neurons were stimulated 24 hours after isolation. Half of the volume (50 µl) was removed from the culture well, mixed with the compound in 96-well V-bottom plates, and added back to the same well. Controls were treated the same way but mixed with solvent only. The cells were fixed by adding 100 µl 8% PFA [final concentration (f.c.) 4%] for 10 minutes at RT. Stimulations were performed in a heated (37℃) water bath or within the incubator. Neurons were stimulated with the compounds and concentrations as indicated in the text and reagents section.

Immunofluorescence staining

After blocking and permeabilization (2% goat serum, 1% BSA, 0.1% Triton X-100, 0.05% Tween 20 for 1 hour, at RT), sections or cells were incubated with primary antibodies in 1% BSA in PBS at 4℃ overnight. After three washes with PBS (10 minutes, RT), cells were incubated with secondary antibodies (1:1000, 1 hour, RT). After three final washes (30 minutes, RT), the plates were stored at 4℃ until scanning. Sections were mounted with Fluoromount-G (Southern Biotech). Refer to antibodies section for dilutions.

Quantitative microscopy

Stained cultures in 96-well plates were scanned using a Cellomics ArrayScan VTI. Images of 512×512 pixels were acquired with a 10× objective and analyzed using the Cellomics software package. Briefly, images of UCHL1 stainings were background corrected (low pass filtration), converted to binary image masks (fixed threshold), segmented (geometric method), and neurons were identified by the object selection parameters – size: 120–4000 μm^2; circularity (perimeter^2/4π area): 1–2; length-to-width ratio: 1–2; average intensity: 250–2000; total intensity: 6×10^4–5×10^6. The image masks were then used to quantify signals in other channels. For dose–response and time course experiments, raw mean values of triplicate samples were normalized to a mean baseline value from all untreated wells. Bleed-through was compensated as described previously (Roederer, 2002). Probability density plots were generated using the *R* package (1D plots) or FlowJo (2D plots). Gating of subpopulations was performed either by setting thresholds at local minima of probability density plots or using threshold free mixture modeling (see below).

Calcium imaging followed by quantitative microscopy

DRG neurons were plated in 348-well glass-bottomed plates (Greiner; 1000 neurons/well, 80 µl medium) and cultured overnight. Neuron cultures were loaded with 0.005 µg/µl FURA-2-AM (Invitrogen) in Neurobasal-A/B27 medium for 40 minutes and washed twice with medium for 10 minutes. Calcium traces were recorded with the Cellomics Arrayscan VTI. Calcium influx was induced by automatically dispensing 5 µl capsaicin (f.c. 250 nM) or KCl (f.c. 30 mM) with the Arrayscans computer-controlled pipettor. Cells were

fixed with 2% PFA for 20 minutes and immunostained for the respective markers as described above, outside the microscope. All wells were then imaged again with the Arrayscan VTI. Using ImageJ, UCHL1 images were background corrected (rolling ball), converted to binary image masks (Li thresholding), segmented (water shed), and objects were identified by their circularity (4π area/perimeter^2=0.5–1) and size (120–4000 μm^2). The single cell masks were then used to determine 340/380 nm values as well as RIIβ and UCHL1 expression levels for each cell. Then the average calcium traces were calculated for the RIIβ(+) and the RIIβ(−) neurons. Average traces of three experiments (means ± s.e.m.) are shown. Living neurons showed a response >25% over the baseline to either capsaicin or KCl.

Mixture modeling of stimulus experiments

The gamma probability distribution, given by the density function:

$$p(x) = 1/\left(\Gamma(k)\theta^k\right)x^{k-1}e^{-\frac{x}{\theta}} \quad (1)$$

with shape parameter k, scale parameter θ, and γk the gamma function, has been previously suggested as a model for the intracellular distribution of proteins (Friedman et al., 2006). Population data from control experiments were fitted with a gamma distribution by adjusting the parameters k and θ using a maximum-likelihood approach (Choi and Wette, 1969). For each stimulus experiment a mixture model composed of two gamma distributions was computed. The first mixture component was fixed to the distribution obtained from the control experiment, and the second component was chosen as another gamma distribution with adjustable parameters. The parameters and the component weights were optimized with the expectation maximization algorithm implemented in the software library 'PyMix' (Georgi et al., 2010). We used a standard hypothesis test based on the likelihood ration to test whether the population model of two gamma distributed subpopulations was statistically significant compared with a model with a single gamma distribution. The null hypothesis was that the population is described by a single gamma distribution, and the alternative hypothesis is that the population is a mixture of two gamma distributions. We used the test statistic $T=-2\log L$, where L is the likelihood ratio of the null hypothesis model versus the mixture model (Koch, 2010). For large sample sizes, the test statistic T is chi-square distributed, and a significance level of $P=0.001$ is achieved for $T\geq 10.83$. We judged the partitioning as statistically significant, if $T\geq 10.83$ in each of the three replicates of an experiment.

BRET assay

F11 cells were seeded in 96-well plates (Nunc) coated with collagen (Roche) at a density of 1.5×10^4 cells/well and cultured in Hams F-12 medium (Sigma-Aldrich) with 15% FCS (PAA) and 1% penicillin and streptomycin (PAA). The cells were transfected after 24 hours using Lipofectamine 2000 (Invitrogen). Cells were rinsed with PBS 48 hours later, treated with the respective reagents for 20 minutes, and the substrate coelenterazine 400a (Biotrend) was added at a final concentration of 5 µM in a total volume of 30 µl PBS prior to the BRET measurement. Light emission was detected with a POLARstar Omega microplate reader (BMG Labtech). For each well the light output was taken simultaneously using filters at the wavelengths 410 nm (±80 nm) for the donor and 515 nm (±30 nm) for the acceptor. Emission values obtained with untransfected (n.t.) cells were subtracted, and BRET signals were calculated as follows: [emission (515 nm)−n.t. cells (515 nm)]/[emission (410 nm)−n.t. cells (410 nm)]. Control measurements with cells expressing RLuc alone were included in each experiment.

Acknowledgements

We thank Prof. Ropers for supporting this work and Vanessa Suckow for outstanding technical assistance.

Competing interests

The authors declare no competing interests.

Author contributions

J.I., M.D., A.P., F.H. and T.H. conceived and designed the experiments. J.I., M.D. and R.B. performed the experiments. J.I., M.D., R.B., S.W., J.H. and F.A. analyzed the data. J.I., T.H. and F.H. wrote the paper.

Funding

This work was supported by the Bundesministerium für Bildung und Forschung projects 'Modelling pain switches (MoPS)' (FKZ0315449D) and NoPain (FKZ0316177A, FKZ0316177FF) as well as by the European Union FP7 collaborative project Affinomics [contract number 241481 to F.W.H.].

References

Amieux, P. S., Cummings, D. E., Motamed, K., Brandon, E. P., Wailes, L. A., Le, K., Idzerda, R. L. and McKnight, G. S. (1997). Compensatory regulation of RIalpha protein levels in protein kinase A mutant mice. *J. Biol. Chem.* **272**, 3993-3998.

Amieux, P. S., Howe, D. G., Knickerbocker, H., Lee, D. C., Su, T., Laszlo, G. S., Idzerda, R. L. and McKnight, G. S. (2002). Increased basal cAMP-dependent protein kinase activity inhibits the formation of mesoderm-derived structures in the developing mouse embryo. *J. Biol. Chem.* **277**, 27294-27304.

Basbaum, A. I., Bautista, D. M., Scherrer, G. and Julius, D. (2009). Cellular and molecular mechanisms of pain. *Cell* **139**, 267-284.

Belmonte, C. and Viana, F. (2008). Molecular and cellular limits to somatosensory specificity. *Mol. Pain* **4**, 14.

Bhave, G., Zhu, W., Wang, H., Brasier, D. J., Oxford, G. S. and Gereau, R. W., 4th (2002). cAMP-dependent protein kinase regulates desensitization of the capsaicin receptor (VR1) by direct phosphorylation. *Neuron* **35**, 721-731.

Boettcher, A. J., Wu, J., Kim, C., Yang, J., Bruystens, J., Cheung, N., Pennypacker, J. K., Blumenthal, D. A., Kornev, A. P. and Taylor, S. S. (2011). Realizing the allosteric potential of the tetrameric protein kinase A RIα holoenzyme. *Structure* **19**, 265-276.

Brandon, E. P., Logue, S. F., Adams, M. R., Qi, M., Sullivan, S. P., Matsumoto, A. M., Dorsa, D. M., Wehner, J. M., McKnight, G. S. and Idzerda, R. L. (1998). Defective motor behavior and neural gene expression in RIIbeta-protein kinase A mutant mice. *J. Neurosci.* **18**, 3639-3649.

Cadd, G. and McKnight, G. S. (1989). Distinct patterns of cAMP-dependent protein kinase gene expression in mouse brain. *Neuron* **3**, 71-79.

Choi, S. C. and Wette, R. (1969). Maximum likelihood estimation of the parameters of the gamma distribution and their bias. *Technometrics* **11**, 683-690.

Cummings, D. E., Brandon, E. P., Planas, J. V., Motamed, K., Idzerda, R. L. and McKnight, G. S. (1996). Genetically lean mice result from targeted disruption of the RII beta subunit of protein kinase A. *Nature* **382**, 622-626.

Diskar, M., Zenn, H. M., Kaupisch, A., Prinz, A. and Herberg, F. W. (2007). Molecular basis for isoform-specific autoregulation of protein kinase A. *Cell. Signal.* **19**, 2024-2034.

England, S., Bevan, S. and Docherty, R. J. (1996). PGE2 modulates the tetrodotoxin-resistant sodium current in neonatal rat dorsal root ganglion neurones via the cyclic AMP-protein kinase A cascade. *J. Physiol.* **495**, 429-440.

Fischer, Q. S., Beaver, C. J., Yang, Y., Rao, Y., Jakobsdottir, K. B., Storm, D. R., McKnight, G. S. and Daw, N. W. (2004). Requirement for the RIIbeta isoform of PKA, but not calcium-stimulated adenylyl cyclase, in visual cortical plasticity. *J. Neurosci.* **24**, 9049-9058.

Fitzgerald, E. M., Okuse, K., Wood, J. N., Dolphin, A. C. and Moss, S. J. (1999). cAMP-dependent phosphorylation of the tetrodotoxin-resistant voltage-dependent sodium channel SNS. *J. Physiol.* **516**, 433-446.

Friedman, N., Cai, L. and Xie, X. S. (2006). Linking stochastic dynamics to population distribution: an analytical framework of gene expression. *Phys. Rev. Lett.* **97**, 168302.

Georgi, B., Costa, I. G. and Schliep, A. (2010). PyMix—the python mixture package—a tool for clustering of heterogeneous biological data. *BMC Bioinformatics* **11**, 9.

Huang, Y. Y., Kandel, E. R., Varshavsky, L., Brandon, E. P., Qi, M., Idzerda, R. L., McKnight, G. S. and Bourtchouladze, R. (1995). A genetic test of the effects of mutations in PKA on mossy fiber LTP and its relation to spatial and contextual learning. *Cell* **83**, 1211-1222.

Hucho, T. and Levine, J. D. (2007). Signaling pathways in sensitization: toward a nociceptor cell biology. *Neuron* **55**, 365-376.

Inan, M., Lu, H. C., Albright, M. J., She, W. C. and Crair, M. C. (2006). Barrel map development relies on protein kinase A regulatory subunit II beta-mediated cAMP signaling. *J. Neurosci.* **26**, 4338-4349.

Jeske, N. A., Diogenes, A., Ruparel, N. B., Fehrenbacher, J. C., Henry, M., Akopian, A. N. and Hargreaves, K. M. (2008). A-kinase anchoring protein mediates TRPV1 thermal hyperalgesia through PKA phosphorylation of TRPV1. *Pain* **138**, 604-616.

Ji, R. R., Kohno, T., Moore, K. A. and Woolf, C. J. (2003). Central sensitization and LTP: do pain and memory share similar mechanisms? *Trends Neurosci.* **26**, 696-705.

Kim, C., Cheng, C. Y., Saldanha, S. A. and Taylor, S. S. (2007). PKA-I holoenzyme structure reveals a mechanism for cAMP-dependent activation. *Cell* **130**, 1032-1043.

Journal of Cell Science

Kim, H. Y., Lee, K. Y., Lu, Y., Wang, J., Cui, L., Kim, S. J., Chung, J. M. and Chung, K. (2011). Mitochondrial Ca(2+) uptake is essential for synaptic plasticity in pain. *J. Neurosci.* **31**, 12982-12991.

Koch, K. R. (2010). *Parameter Estimation and Hypothesis Testing in Linear Models*. Berlin: Springer-Verlag.

Malmberg, A. B., Brandon, E. P., Idzerda, R. L., Liu, H., McKnight, G. S. and Basbaum, A. I. (1997). Diminished inflammation and nociceptive pain with preservation of neuropathic pain in mice with a targeted mutation of the type I regulatory subunit of cAMP-dependent protein kinase. *J. Neurosci.* **17**, 7462-7470.

Manni, S., Mauban, J. H., Ward, C. W. and Bond, M. (2008). Phosphorylation of the cAMP-dependent protein kinase (PKA) regulatory subunit modulates PKA-AKAP interaction, substrate phosphorylation, and calcium signaling in cardiac cells. *J. Biol. Chem.* **283**, 24145-24154.

Martin, B. R., Deerinck, T. J., Ellisman, M. H., Taylor, S. S. and Tsien, R. Y. (2007). Isoform-specific PKA dynamics revealed by dye-triggered aggregation and DAKAP1alpha-mediated localization in living cells. *Chem. Biol.* **14**, 1031-1042.

Moriyama, T., Higashi, T., Togashi, K., Iida, T., Segi, E., Sugimoto, Y., Tominaga, T., Narumiya, S. and Tominaga, M. (2005). Sensitization of TRPV1 by EP1 and IP reveals peripheral nociceptive mechanism of prostaglandins. *Mol. Pain* **1**, 3.

Murata, T., Ushikubi, F., Matsuoka, T., Hirata, M., Yamasaki, A., Sugimoto, Y., Ichikawa, A., Aze, Y., Tanaka, T., Yoshida, N. et al. (1997). Altered pain perception and inflammatory response in mice lacking prostacyclin receptor. *Nature* **388**, 678-682.

Oliveria, S. F., Dell'Acqua, M. L. and Sather, W. A. (2007). AKAP79/150 anchoring of calcineurin controls neuronal L-type Ca2+ channel activity and nuclear signaling. *Neuron* **55**, 261-275.

Pidoux, G. and Taskén, K. (2010). Specificity and spatial dynamics of protein kinase A signaling organized by A-kinase-anchoring proteins. *J. Mol. Endocrinol.* **44**, 271-284.

Pierre, S., Eschenhagen, T., Geisslinger, G. and Scholich, K. (2009). Capturing adenylyl cyclases as potential drug targets. *Nat. Rev. Drug Discov.* **8**, 321-335.

Prinz, A., Diskar, M., Erlbruch, A. and Herberg, F. W. (2006a). Novel, isotype-specific sensors for protein kinase A subunit interaction based on bioluminescence resonance energy transfer (BRET). *Cell. Signal.* **18**, 1616-1625.

Prinz, A., Diskar, M. and Herberg, F. W. (2006b). Application of bioluminescence resonance energy transfer (BRET) for biomolecular interaction studies. *ChemBioChem* **7**, 1007-1012.

Pulichino, A. M., Rowland, S., Wu, T., Clark, P., Xu, D., Mathieu, M. C., Riendeau, D. and Audoly, L. P. (2006). Prostacyclin antagonism reduces pain and inflammation in rodent models of hyperalgesia and chronic arthritis. *J. Pharmacol. Exp. Ther.* **319**, 1043-1050.

Rangel-Aldao, R. and Rosen, O. M. (1976). Dissociation and reassociation of the phosphorylated and nonphosphorylated forms of adenosine 3′:5′ -monophosphate-dependent protein kinase from bovine cardiac muscle. *J. Biol. Chem.* **251**, 3375-3380.

Rangel-Aldao, R., Kupiec, J. W. and Rosen, O. M. (1979). Resolution of the phosphorylated and dephosphorylated cAMP-binding proteins of bovine cardiac muscle by affinity labeling and two-dimensional electrophoresis. *J. Biol. Chem.* **254**, 2499-2508.

Rao, Y., Fischer, Q. S., Yang, Y., McKnight, G. S., LaRue, A. and Daw, N. W. (2004). Reduced ocular dominance plasticity and long-term potentiation in the developing visual cortex of protein kinase A RII alpha mutant mice. *Eur. J. Neurosci.* **20**, 837-842.

Rathee, P. K., Distler, C., Obreja, O., Neuhuber, W., Wang, G. K., Wang, S. Y., Nau, C. and Kress, M. (2002). PKA/AKAP/VR-1 module: A common link of Gs-mediated signaling to thermal hyperalgesia. *J. Neurosci.* **22**, 4740-4745.

Reinold, H., Ahmadi, S., Depner, U. B., Layh, B., Heindl, C., Hamza, M., Pahl, A., Brune, K., Narumiya, S., Müller, U. et al. (2005). Spinal inflammatory hyperalgesia is mediated by prostaglandin E receptors of the EP2 subtype. *J. Clin. Invest.* **115**, 673-679.

Roederer, M. (2002). Compensation in flow cytometry. *Curr. Protoc. Cytom.* **22**, 1.14.1–1.14.20.

Schnizler, K., Shutov, L. P., Van Kanegan, M. J., Merrill, M. A., Nichols, B., McKnight, G. S., Strack, S., Hell, J. W. and Usachev, Y. M. (2008). Protein kinase A anchoring via AKAP150 is essential for TRPV1 modulation by forskolin and prostaglandin E2 in mouse sensory neurons. *J. Neurosci.* **28**, 4904-4917.

Taylor, S. S., Buechler, J. A. and Yonemoto, W. (1990). cAMP-dependent protein kinase: framework for a diverse family of regulatory enzymes. *Annu. Rev. Biochem.* **59**, 971-1005.

Taylor, S. S., Ilouz, R., Zhang, P. and Kornev, A. P. (2012). Assembly of allosteric macromolecular switches: lessons from PKA. *Nat. Rev. Mol. Cell Biol.* **13**, 646-658.

Thiele, T. E., Willis, B., Stadler, J., Reynolds, J. G., Bernstein, I. L. and McKnight, G. S. (2000). High ethanol consumption and low sensitivity to ethanol-induced sedation in protein kinase A-mutant mice. *J. Neurosci.* **20**, RC75.

Vigil, D., Blumenthal, D. K., Taylor, S. S. and Trewhella, J. (2006). Solution scattering reveals large differences in the global structures of type II protein kinase A isoforms. *J. Mol. Biol.* **357**, 880-889.

Wang, C., Li, G. W. and Huang, L. Y. (2007). Prostaglandin E2 potentiation of P2X3 receptor mediated currents in dorsal root ganglion neurons. *Mol. Pain* **3**, 22.

Wu, J., Brown, S. H., von Daake, S. and Taylor, S. S. (2007). PKA type IIalpha holoenzyme reveals a combinatorial strategy for isoform diversity. *Science* **318**, 274-279.

Zhang, J., Hupfeld, C. J., Taylor, S. S., Olefsky, J. M. and Tsien, R. Y. (2005). Insulin disrupts beta-adrenergic signalling to protein kinase A in adipocytes. *Nature* **437**, 569-573.

Zhang, X., Li, L. and McNaughton, P. A. (2008). Proinflammatory mediators modulate the heat-activated ion channel TRPV1 via the scaffolding protein AKAP79/150. *Neuron* **59**, 450-461.

Zhang, P., Smith-Nguyen, E. V., Keshwani, M. M., Deal, M. S., Kornev, A. P. and Taylor, S. S. (2012). Structure and allostery of the PKA RIIβ tetrameric holoenzyme. *Science* **335**, 712-716.

Zimmermann, B., Chiorini, J. A., Ma, Y., Kotin, R. M. and Herberg, F. W. (1999). PrKX is a novel catalytic subunit of the cAMP-dependent protein kinase regulated by the regulatory subunit type I. *J. Biol. Chem.* **274**, 5370-5378.